Structural environment and oxidation state of Mn in goethic-groutite solid-solutions

Article *in* American Mineralogist · January 2001

DOI: 10.2138/am-2001-0115

5 authors, including:

Andreas C Scheinost
Helmholtz-Zentrum Dresden-Rossendorf
279 PUBLICATIONS **8,314** CITATIONS
SEE PROFILE

Helge Stanjek
RWTH Aachen University
148 PUBLICATIONS **4,419** CITATIONS
SEE PROFILE

Darrell Schulze
Purdue University
91 PUBLICATIONS **3,709** CITATIONS
SEE PROFILE

Ubald Gasser
Amt für Landschaft und Natur
14 PUBLICATIONS **542** CITATIONS
SEE PROFILE

American Mineralogist, Volume 86, pages 139–146, 2001

Structural environment and oxidation state of Mn in goethite-groutite solid-solutions

ANDREAS C. SCHEINOST,[1,*] HELGE STANJEK,[2] DARRELL G. SCHULZE,[3] UBALD GASSER,[4] AND DONALD L. SPARKS[1]

[1]Department of Plant and Soil Sciences, University of Delaware, Newark, Delaware 19717-1303, U.S.A.
[2]Lehrstuhl für Bodenkunde, Technische Universität, München, 85350 Freising, Germany
[3]Agronomy Department, Purdue University, West Lafayette, Indiana 47907, U.S.A.
[4]College of Engineering ISW, P.O. Box 335, CH 8820 Wadenswil, Switzerland

ABSTRACT

Both X-ray absorption and diffraction techniques were used to study the structural environment and oxidation state of Mn in goethite-groutite solid solutions, α-$Mn_xFe_{1-x}OOH$, with $x_{Mn} \leq 0.47$. Rietveld refinement of X-ray diffraction (XRD) data was employed to investigate the statistical long-range structure. The results suggest that increasing x_{Mn} leads to a gradual elongation of Fe and Mn occupied octahedra which, in turn, causes a gradual increase of the lattice parameter *a* and a gradual decrease of *b* and *c* in line with Vegard's law. X-ray absorption fine structure (XAFS) spectra at the Mn*K*α and Fe*K*α edges revealed, however, that the local structure around Fe remains goethite-like for $x_{Mn} \leq 0.47$, while the local structure around Mn is goethite-like for $x_{Mn} \leq 0.13$, but groutite-like for higher x_{Mn}. The spectral observations were confirmed by XAFS-derived metal distances showing smaller changes around Fe and larger changes around Mn as compared with those determined by XRD. Therefore, the XAFS results indicate formation of groutite-like clusters in the goethite host structure for $x_{Mn} > 0.13$, which remain undetected by XRD. The first prominent resonance peak in the X-ray absorption near-edge spectra (XANES) of the Mn goethites was 17.2 to 17.8 eV above the Fermi level of Mn (6539 eV), in line with that of Mn^{3+} reference compounds, and well separated from that of Mn^{2+} and Mn^{4+} compounds. Therefore, Mn in goethite is dominantly trivalent regardless of whether the samples were derived from Mn^{2+} or Mn^{3+} solutions. This may indicate a catalytic oxidation of Mn^{2+} during goethite crystal growth similar to that found at the surface of Mn oxides.

INTRODUCTION

Goethite, α-FeOOH, is the most ubiquitous iron oxide in terrestrial soils (Cornell and Schwertmann 1996). In natural goethites, Al frequently substitutes for Fe, occasionally reaching up to 0.33 mole fractions (Fitzpatrick and Schwertmann 1982; Tardy and Nahon 1985; Fabris et al. 1986; Carlson 1995). Although V^{3+}, Cr^{3+}, Mn^{3+}, Co^{2+}, Ni^{2+}, Cu^{2+}, and Zn^{2+} have ionic radii and electronic configurations much more similar to Fe than Al, transition metal substituted goethites are less commonly found in soils (Anand and Gilkes 1987; Trolard et al. 1989; Singh and Gilkes 1992; Schwertmann and Pfab 1997). For all except Mn, this can be explained by their low abundance in the Earth's crust (<135 mg/kg) and by their tendency to form minerals with a high weathering stability (Mason and Moore 1982). Manganese, however, is much more common (~950 mg/kg), and it is mobilized and precipitated in soils and sediments together with Fe over a similar range of redox potentials (Patrick and Jugsujinda 1992). Surprisingly, reports on Mn-substituted goethite, $Mn_xFe_{1-x}OOH$ are scarce, either from soils (Vandenberghe et al. 1986a; Hus and Stiers 1987; Trolard et al. 1995) or from marine crusts (Boughriet et al. 1996). One so-called Mn goethite from a deep-sea Fe-Mn crust contained Mn^{4+}, and most likely as a separate Mn phase associated with goethite instead of being a Mn substituted goethite (Manceau et al. 1992). In manganese nodules with a wide elemental variation in distinct growth bands, the presence of higher concentrations of Mn even seemed to exclude Fe, and vice versa (Burns and Burns 1979). In the laboratory, however, α-$Mn_xFe_{1-x}OOH$ can be easily synthesized from Mn^{3+} or Mn^{2+} salts, with x_{Mn} up to 0.13 (Stiers and Schwertmann 1985; Vandenberghe et al. 1986b; Cornell and Giovanoli 1987a; Diaz et al. 1989; Vempati et al. 1995; Ford et al. 1997; Gasser et al. 1999). By sustaining a pH of 6 during crystallization, x_{Mn} as high as 0.47 could be achieved (Ebinger and Schulze 1989, 1990). Ferrimagnetic (Fe, Mn) spinel phases form, however, at a pH of 8 or higher (Ebinger and Schulze 1990; Wolski et al. 1997).

Although the α-MnOOH end-member, groutite, occurs in marine environments and ore bodies (Varentsov 1996), it has not been found in soils, where Mn^{4+} oxides or mixed Mn^{4+}/Mn^{3+} oxides, like birnessite, lithiophorite, hollandite, pyrolusite, todorokite, romanèchite, vernadite, and cryptomelane are prevalent (Taylor et al. 1964; Ross et al. 1976; Uzochukwu and Dixon 1986; Birnie and Paterson 1991; Robbins et al. 1993). The nomi-

* Present address: Institute of Terrestrial Ecology, ETHZ, CH 8952 Schlieren, Switzerland.
E-mail: scheinost@ito.umnw.ethz.ch

nal oxidation states of these minerals have been confirmed by XANES (Manceau et al. 1992). XANES of moist topsoils detected only Mn^{2+} and Mn^{4+} (Schulze et al. 1995).

There are several possible reasons for the rarity of α-$Mn_xFe_{1-x}OOH$ in natural systems. The aqueous Mn^{3+} species readily disproportionates to Mn^{2+} and Mn^{4+} (ΔG^0_{298} = –109 kJ/mol) (Stumm and Morgan 1970; Burns 1993), and the dominant mobile form, Mn^{2+}, readily oxidizes at the surface of minerals (Junta and Hochella 1994) or bacteria directly to Mn^{4+} without an intermediate Mn^{3+} step (Mandernack et al. 1995). These reactions should limit the source of Mn^{2+} and Mn^{3+}, which are necessary precursors for the formation of $Mn_xFe_{1-x}OOH$. However, aqueous Mn^{2+} sorbs onto previously precipitated Mn minerals and oxidizes in a catalytic surface reaction to Mn^{3+} (Murray et al. 1985). At pH 6, groutite precipitates formed from aqueous Mn^{2+} at the surface of birnessite (Tu et al. 1994), confirming pH to be a key variable for the preferential formation of groutite over other Mn minerals (Cornell and Giovanoli 1987a; Ebinger and Schulze 1990).

The oxidation state of Mn in a particular mineral depends on the oxidation potential of the solution and the structure of the mineral. The latter aspect determines the ligand field affecting Mn, and, in turn, its relative crystal field stabilization energy (CFSE). In octahedral symmetry the CFSE increases from Mn^{2+} (CFSE = 0) to Mn^{3+} (CFSE = 3/5·10Dq) to Mn^{4+} (6/5·10Dq) (Burns 1993). This may explain the prevalence of Mn^{4+} in those minerals, which are able to host Mn in several oxidation states (Manceau et al. 1992; Nesbitt and Banerjee 1998). Due to the $(t_{2g})^3$ $(e_g)^1$ configuration, however, Mn^{3+} minerals are susceptible to the Jahn-Teller distortion, which decreases the symmetry of the octahedra from O_h to D_{4h}. The resulting increase of CFSE may also stabilize Mn^{3+} in such minerals. Once groutite has formed, it should persist in spite of its metastability relative to the more common manganite, γ-MnOOH, because of the small enthalpy gradient between groutite and manganite (Fritsch et al. 1997).

The degeneracy of the Mn^{3+} electron ground state may be removed by either octahedral compression or elongation. However, most Mn^{3+} minerals, including groutite, show an elongation (Hoffmann et al. 1997). Ebinger and Schulze (1989) concluded that the increase in *a* and the decrease in *b* and *c* of Mn-substituted goethite were due to this elongation of the Mn octahedra, hence indirectly proving the stabilization of Mn^{3+} in goethite. Other authors pointed out, however, that the elongation of the $Mn(O,OH)_6$ octahedra would cause structural incompatibility with the shorter $Fe(O,OH)_6$ octahedra, thus limiting the extent to which the $Mn_xFe_{1-x}OOH$ solid solution would be stable (Manceau et al. 1992).

The objective of our work is (1) to confirm the trivalent oxidation state of Mn in goethite and (2) to investigate whether the composition of the two different structures is accompanied by a random distribution of Mn among the Fe sites or by some degree of clustering. We used Rietveld refinements of X-ray diffraction (XRD) patterns to model the structure of $Mn_xFe_{1-x}OOH$. Because Mn and Fe scatter very similarly and occupy the same 4c site, only an average (long range) structure can be obtained with this method. Therefore, we used X-ray absorption fine structure (XAFS) spectroscopy at the Fe*K*α and Mn*K*α edge to probe the short-range structure (<8 Å) around Mn and Fe separately and X-ray absorption near edge structure (XANES) spectroscopy to determine the oxidation state of Mn.

Materials and methods

Samples

We used eight synthetic Mn substituted goethites from three synthesis series, with x_{Mn} ranging from 0 to 0.47 (Table 1). Information on the preparation and properties of the series were published elsewhere (Ebinger and Schulze 1990; Vempati et al. 1995; Gasser et al. 1999). Briefly, Ebinger and Schulze (1990) prepared series S250* with x_{Mn} from 0.18 to 0.47 by adding 2 *M* NH_4OH to nitrate solutions of Mn^{2+} and Fe^{3+}. The suspension were aged for 40 days at pH 6 and 50 °C. Gasser et al. (1999) prepared series Mni-* with x_{Mn} up to 0.13 using a similar method, but aging was at pH >13 and 63 ºC for 15 days. Vempati et al. (1995) prepared series MnGt* starting from chloride solutions of Mn^{3+} and Fe^{3+}, and the suspensions were aged for 24 hours at 70 °C. From XRD, all Mn specimens contained only goethite. An unsubstituted goethite sample (G39/25.3) synthesized at 25 °C (Schwertmann et al. 1985), and a natural sample of groutite (α-MnOOH) from Louise Pit, Minnesota (no. 138621 Smithsonian Institution), represent the end-member phases. The groutite sample contained 40% manganite (see XRD results below).

X-ray diffraction

The samples were mixed with varying quantities of Si as an internal standard and scanned from 4 to 93° 2θ with 0.015° steps and 10 s counting time using Mo or Co*K*α radiation and a Philipps PW1820 goniometer equipped with a diffracted beam monochromator. Due to pronounced asymmetry at low diffraction angles, the structural refinements with the PowerPC version of RIETAN (Izumi 1993) were performed from 2θ = 14 to 93° (2.91 > *d* > 0.489 Å). The profiles were modeled with the Thompson-Cox-Hastings function (Thompson et al. 1987) in which the Gaussian and the Lorentzian components are refined separately. The Gaussian component of the integral breadth was constrained with the Caglioti formula (Caglioti et al. 1958). The Lorentzian component was split into a Scherrer term ($X \sim 1/\cos\theta$) and X_e, and a strain term ($Y \sim \tan\theta$). The unit-cell lengths (Si and goethite), the preferred orientation (March-Dollase), the isotropic temperature factors, and the site coordinates were refined. The goethite unit-cell lengths were recalculated after correcting 2θ by reference to the ideal unit-cell length of the Si internal standard (a_0 = 5.43094 Å). Bond lengths and angles were calculated with ATOMS 4.1 (Shape Software, Kingsport, Tennessee).

X-ray absorption fine structure spectroscopy

XAFS spectra at the Mn*K*α and at the Fe*K*α edge were recorded in transmission mode at beamline X-11A, National Synchrotron Light Source (NSLS), Brookhaven National Laboratory. The electron storage ring was operated at 2.8 GeV. A Si [111] monochromator crystal was detuned by 25% for harmonic rejection. The goniometer position was calibrated using Mn and Fe foils, assigning E_0 = 6539 eV for Mn and E_0 = 7112 eV for Fe to the first inflexion point of the absorption

TABLE 1. Sample description, Mn-XANES edge position, and results from the Rietveld refinement (space group *Pnma*)

Sample	x_{Mn}	XANES	UCL			Atomic positions						Statistics			
		(eV)	a_0 (Å)	b_0 (Å)	c_0 (Å)	Fe_x	Fe_z	$O1_x$	$O1_z$	$O2_x$	$O2_z$	B_{Fe}	B_O	*Rwp*	*S*
G39/25.3	0.000	–	9.9600	3.0239	4.6092	0.1461	–0.0477	–0.1994	0.2942	–0.0531	–0.19740	0.62	0.44	6.7	2.2
Mni-7	0.005	17.8	9.9610	3.0251	4.6162	0.1458	–0.0480	–0.2001	0.2867	–0.0544	–0.18430	0.61	0.28	6.7	2.3
MnGt02	0.007	17.8	9.9607	3.0258	4.6060	0.1453	–0.0490	–0.1994	0.2875	–0.0593	–0.18180	0.76	0.55	8.6	3.5
Mni-2	0.050	17.8	9.9702	3.0226	4.6076	0.1453	–0.0486	–0.2003	0.2869	–0.0549	–0.18250	0.61	0.39	6.9	2.4
MnGt08	0.061	17.4	9.9720	3.0209	4.6026	0.1450	–0.0490	–0.1996	0.2886	–0.0566	–0.18730	0.74	0.59	7.1	2.8
Mni-6	0.125	17.4	9.9908	3.0150	4.5971	0.1443	–0.0488	–0.1999	0.2887	–0.0570	–0.18470	0.55	0.48	7.2	2.7
S2502	0.180	17.2	10.1155	2.9897	4.5812	0.1406	–0.0482	–0.2002	0.3037	–0.0619	–0.19650	0.87	0.65	8.7	3.0
S2504	0.350	17.5	10.2499	2.9582	4.5745	0.1408	–0.0496	–0.1946	0.2992	–0.0621	–0.19800	0.87	0.82	8.1	2.8
S2508	0.470	17.5	10.3827	2.9351	4.5626	0.1384	–0.0495	–0.1972	0.2825	–0.0607	–0.18740	0.83	1.48	9.2	3.3
Groutite	1.000	17.6	10.6908	2.8753	4.5612	0.1397	–0.0484	–0.1807	0.3140	–0.0814	–0.18299	0.85	0.93	8.2	2.3

Note: XANES is the position of the first resonance peak above the Mn*K*α edge, given in eV relative to the Fermi level. UCL is unit cell length; B_{Fe} and B_O are the isotropic temperature factors of Fe and O, respectively; *S* is the goodness of fit. All numbers have statistically significant digits only.

edges. Incident and transmitted X-ray fluxes were measured with He/N_2-filled ionization chambers. Spectra at the Fe*K*α edge were recorded relative to E_0 with the following parameters: –200 to –30 eV in 10 eV steps and 1σ integration time; –30 to 30 eV in 0.5 eV steps at 0.5 s; 30 eV to 15 $Å^{-1}$ in 0.05 $Å^{-1}$ steps at 4 s. The Mn*K*α spectra of the Fe containing samples were collected up to 12 $Å^{-1}$ only because of the subsequent Fe edge. At least three individual spectra were recorded and averaged.

The XAFS data reduction was performed with WinXAS 97 version 1.3 written by Thorsten Ressler. Spectra were normalized by fitting second degree polynomial functions to the preedge and the XAFS region. E_0 was set to the first of two inflexion points in the main edge. After conversion into k space, the XAFS oscillations were separated by using six spline sections between 1.8 to 2.2 $Å^{-1}$ and 12.0 $Å^{-1}$. To compensate for the attenuation of the amplitude at high *k*, spectra were weighed by k^3. Radial structure functions (RSF) were calculated using a Bessel window for smoothing both ends of the scans.

Theoretical paths were calculated with ATOMS and FEFF7 (Ankudinov and Rehr 1997) using the end-member structures of goethite, α-FeOOH (Forsyth et al. 1968), and groutite, α-MnOOH (Dent Glasser and Ingram 1968). Curved-wave, multiple scattering c(*k*) functions were computed using clusters of ca. 180 atoms ($R_{max} \approx 8$ Å). Since preliminary tests showed that the theoretical backscattering paths from Mn and Fe were almost identical, no further effort was made to create clusters of mixed Fe/Mn composition. The short-range structure around Mn and Fe was modeled by multishell fits to the RSF. Amplitude reduction factors of 0.70 and 0.85 were used for Fe and Mn, respectively. All single shells of a spectrum were fitted with one adjustment of E_0, ΔE_0.

X-ray absorption near-edge structure spectroscopy

XANES spectra were obtained at the X-ray fluorescence microprobe beam line X-26A at the National Synchrotron Light Source (NSLS), Brookhaven National Laboratory, Upton, New York. Technical details of the beam line are given by Schulze et al. (1995) and Bajt et al. (1993). The energy resolution at the Mn edge is ca. 1.5 eV. High-resolution XANES spectra were obtained by scanning the monochromator in 0.5 eV steps across the absorption edge, and in 5 eV steps before and after the edge. Fluorescence was measured with a solid-state detector. Step counting time was varied between 2 and 10 s to give several thousand counts per step above the edge. The energy was calibrated relative to the preedge peak of $KMnO_4$ at 6543.3 eV (Riggs-Gelasco et al. 1996). The samples were diluted with corundum (Buehler Micropolish) to 0.5 to 1 wt% of Mn to avoid self-absorption. The spectra were normalized by fitting first order polynomial functions in the pre-edge range and at 6830 to 6850 eV. Inflexion points and maxima of the edge were determined from cubic-spline first and second derivatives of the spectra.

RESULTS

Oxidation state

Figure 1 compares the XANES spectra of the Mn goethites to those of Mn^{2+} ($MnSO_4$), Mn^{3+} (Mn pyrophosphate, groutite), and Mn^{4+} containing compounds (birnessite and pyrolusite). The first prominent resonance of the Mn goethites is 17.2 to 17.8 eV above the Fermi level at 6539 eV (Table 1), in agreement with the position of groutite (17.6 eV) and close to that of Mn pyrophosphate (16.7 eV). The resonance peak of $MnSO_4$ is significantly ($p < 0.001$) lower at 13.6 eV, and the peaks of pyrolusite (21.1 eV) and birnessite (22.4 eV) are at significantly ($p < 0.001$) higher positions. The observed edge shift is mainly a function of the valence, because the 1s electrons are more tightly bound to the nucleus when the number of valence electrons decreases (Apte and Mande 1982; Calas et al. 1988; Manceau et al. 1992; Schulze et al. 1995; Ammundsen et al. 1996). Thus, the edge position of the Mn-substituted goethites suggests the prevalence of Mn^{3+}.

Long-range structure

The metal octahedra of goethite and groutite share four edges building trans-trans double chains in {010} or b (Fig. 2). Whereas the octahedra of goethite are roughly isometric, the octahedra of groutite are elongated along {100} or a, perpendicular to the chain axis (Hoffmann et al. 1997). Therefore, groutite has a larger *a* and smaller *b* and *c* as compared to goethite (Table 1). In line with previous results, the lattice parameters of Mn goethite show a gradual transition from those of goethite to those of groutite with increasing x_{Mn} (Fig. 3). This Vegard-like behavior of the UCLs has been taken as indication that Mn replaces Fe in the 4c positions of goethite (Ebinger and Schulze 1989; Vempati et al. 1995; Gasser et al. 1999). While *a* and *b* closely adhere to the Vegard line connecting the lattice parameters of the two end-members, *c* decreases faster than predicted, reaching the value of groutite already at $x_{Mn} = 0.5$.

Due to the Rietveld refinement of atomic positions, the

changes on the unit-cell level could be traced back to changes on the level of the fundamental octahedra (Fig. 2). Whereas the two axial Me-(O,OH) distances expand with increasing x_{Mn}, the four equatorial distances remain (O) or decrease (OH) (Fig. 4). This shows that the statistical metal octahedra are increasingly subjected to the Jahn-Teller distortion of Mn^{3+} (Burns 1993). The distances of Mn goethite scatter randomly along the straight lines linking the corresponding end-member distances. Statistical metal-metal distances are also intermediate between those of goethite and groutite (Fig. 5). However, distances between parallel double chains collapse earlier than would be predicted from Vegard's law, causing the fast decrease of *c* shown above. This confirms that the relatively weak hydrogen bonds linking the double chains in *c* are more susceptible to structural changes than the M-O-M bonds (Schulze and Schwertmann 1984).

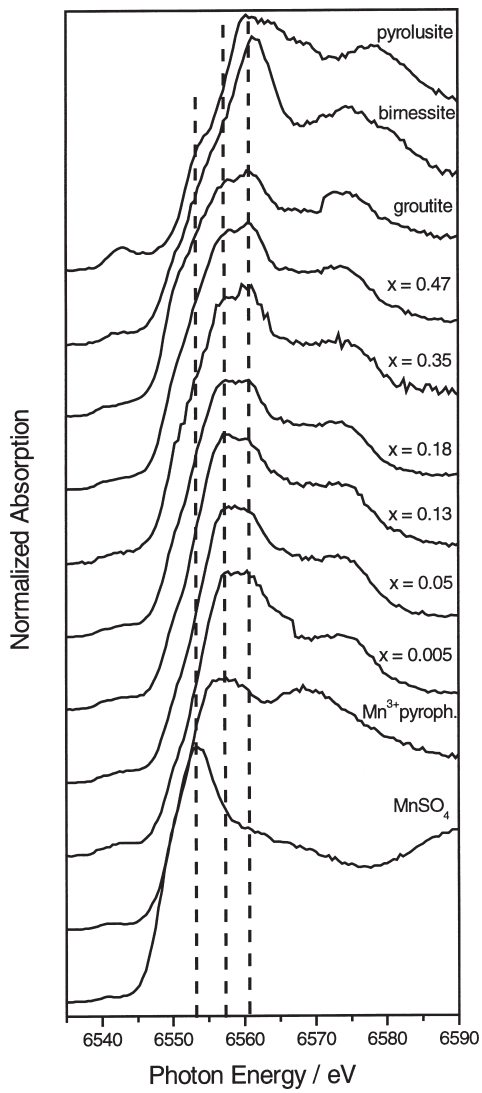

FIGURE 1. XANES of Mn substituted goethites and of reference compounds. The lines mark the position of the first resonance above the Mn*K*α edge for divalent, trivalent, and tetravalent Mn.

Short-range structure

The Rietveld refinement revealed an increasing elongation of metal-$(O,OH)_6$ octahedra with increasing x_{Mn}. As these structural data are statistical averages of many unit cells, it cannot be determined whether the linear changes with x_{Mn} are due to a statistical distribution of Mn over the 4c sites in the goethite structure, or due to groutite-like clusters within the goethite host structure. Preliminary FEFF simulations on mixed clusters of Mn and Fe showed that Mn and Fe in the second shell cannot be distinguished by XAFS, because the backscattering waves are very similar. Thus, a systematic investigation of the degree of clustering as proposed by Waychunas (1983) and Manceau and Calas (1985), which depends on a substantial phase shift between the backscattering waves of the substituting and the replaced metal, could not be performed. However, using XAFS spectroscopy at both the Fe*K*α and the Mn*K*α edge enabled us to probe the local environment of Fe and Mn separately.

The Fe*K*α spectra of select Mn goethite samples and of the goethite reference are shown in Figure 6. The radial structure functions (RSFs), which are uncorrected for phase shift, exhibit a peak at 1.5 Å which is due to backscattering from nearest neighbor O atoms, and a second peak at 2.5 Å which is due to backscattering from the nearest metal atoms. The metal peak has a shoulder on its right wing indicating that it is composed of metal atoms at slightly different distances. With increasing x_{Mn} this shoulder becomes more prominent, while the intensity of the main peak decreases. The χ(k) functions do not show significant changes except for an increase of spectral noise, especially above 10 $Å^{-1}$, with increasing x_{Mn} indicating an increase of structural disorder.

The Mn*K*α spectra of select Mn goethite samples and of the groutite reference are shown in Figure 7. Similar to the spectra at the Fe*K*α edge, the main features of the RSFs are two clearly separated O and metal peaks at low x_{Mn}. A shoulder on the right wing of the metal peak becomes a separate peak for $x_{Mn} > 0.13$. For $x_{Mn} = 0.47$ and the groutite sample, the main metal peak broadened. The χ(*k*) functions fall into two distinct groups, one having a distinct triplet feature between 7.5 to 9.5 $Å^{-1}$ ($x_{Mn} = 0.35$ to 1.00), the other group lacking it ($x_{Mn} = 0.05$ to 0.13). The spectrum at $x_{Mn} = 0.18$ is intermediate and has the lowest noise level. Comparing the respective Fe*K*α and Mn*K*α spectra of four samples (Fig. 8), shows that the local environments of Fe and Mn at x_{Mn} 0.05 and 0.13 are rather similar, but increasingly deviate for higher x_{Mn}. Whereas the local structure of Fe remains goethite-like over the full range of x_{Mn}, the local structure of Mn is goethite-like up to $x_{Mn} = 0.13$, and approaches a groutite-like environment at higher x_{Mn}.

Based on the XRD results, which showed full occupancy of the crystallographic sites of Fe and Mn, we used the crystallographic coordination numbers as fixed input variables for the fit of the XAFS spectra. This allowed us to fit the RSFs with three different metal shells (<4 Å). The shells represent the distance between the metal atoms following each other along the *b* axis (distance 1, CN = 2), the distance between the pairs of metal atoms forming the double chains along *b* (distance 2, CN = 2), and the distance between the two closest metal atoms in neighboring double chains (distance 3, CN = 4) (Fig. 2). The

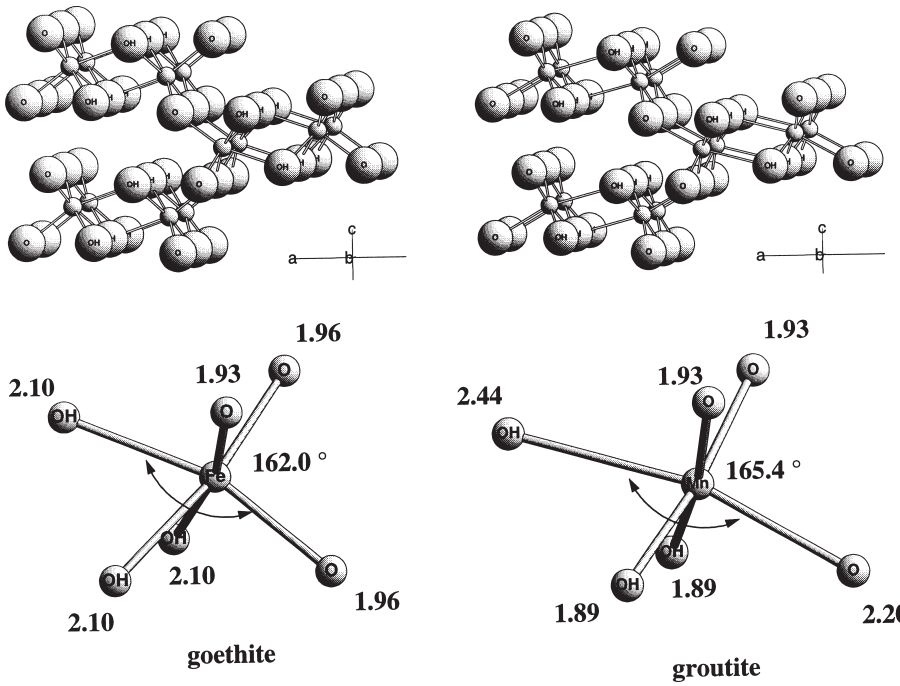

FIGURE 2. Ball-and-stick models of goethite (left side, sample 39/25.3) and groutite (right side). Fe-(O,OH) bond distances (Å), and the angle between the axial ligands are given for single octahedra.

fit results for these three metal shells at the Fe$K\alpha$ and the Mn$K\alpha$ edges are given in Tables 2 and 3. The distances of the three shells are shown in Figure 5 along with the corresponding distances from XRD. Accounting for an absolute error of ±0.01 to ±0.03 Å, the XAFS distances of the end-member phases goethite and groutite are in good agreement with the ones determined by XRD. For both the local structures of Mn and Fe, distance 1 decreases and distance 3 increases with increasing x_{Mn}, in accordance with an increasing Jahn-Teller effect. However, the distortion is much stronger around Mn (relative changes > 0.10 Å between 0.05 and 0.47) than around Fe (relative changes <0.04 Å). At low Mn substitution, the local structure of both Fe and Mn is similar to that of Fe in goethite. At high Mn substitution, the local structure of Mn is similar to that of Mn in groutite, whereas that of Fe is still relatively close to goethite. Thus, the fitted metal distances confirm the spectral observation above.

DISCUSSION

Both the XANES edge position and the Jahn-Teller distortion observed with XRD and XAFS spectroscopy suggest that Mn resides dominantly in its trivalent oxidation state in the Mn goethite samples. However, birnessite contains some Mn^{2+} and up to 33% of Mn^{3+} in addition to the dominant Mn^{4+} (Manceau et al. 1992; Silvester et al. 1997; Nesbitt and Banerjee 1998). This has two implications. First, birnessite is not a perfect standard for Mn^{4+}. Second, we cannot exclude that Mn^{2+} and Mn^{4+} are also present in our Mn goethite samples. To quantify the possible presence of accessory Mn^{2+} and Mn^{4+}, we fitted the edge region of the Mn goethites with linear combinations of the XANES spectra of the reference compounds. In no case was the contribution of the Mn^{2+} or Mn^{4+} standards more than 7%, and the contribution of the Mn^{3+} standard less than 92%. However, this does not necessarily mean that Mn goethite con-

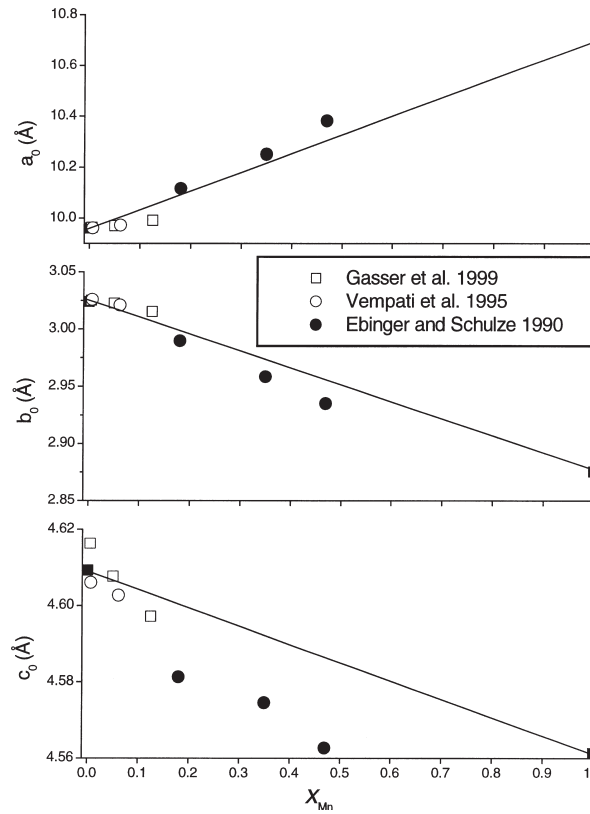

FIGURE 3. Lattice parameters as a function of Mn substitution (space group *Pnma*). The lines link the dimensions of the end-members goethite and groutite (Vegard line).

tains at least 92% of Mn^{3+}. The energy resolution of 1.5 eV at the Mn edge is insufficient to resolve relatively small contributions of other oxidation states (Nesbitt and Banerjee 1998). Furthermore, the XANES main edge is not only influenced by the oxidations state, but also by the local structure of Mn (Manceau et al. 1992). Therefore, it is difficult to estimate whether the changes with x_{Mn} in the XANES of Mn goethites indicate small shifts in oxidation state or whether they are solely due to changes of the local structure.

The dominance of Mn^{3+} in Mn goethite, no matter whether the synthesis started from Mn^{2+} or Mn^{3+}, has two implications. First, the incorporation of trivalent Mn into the growing goethite crystals proceeds faster than Mn^{3+} could dissociate into Mn^{2+} and Mn^{4+}. Second, Mn^{2+} was oxidized, but only by one step to Mn^{3+}. This oxidation reaction may occur at the surface of the growing crystals (Cornell and Giovanoli 1987b; Junta and Hochella 1994), similar to the oxidation of Mn^{2+} at the surface of Mn oxides (Murray et al. 1985; Tu et al. 1994). Thus, trivalent Mn may be more stable and consequently more frequent in the environment than has been assumed earlier.

Due to the Jahn-Teller effect of Mn^{3+}, increasing Mn substitution gradually distorts the long-range structure of goethite toward that of groutite. For $x_{Mn} \leq 0.13$, the statistical long-range structure determined by XRD, and the short-range structure around Fe and Mn were similar. Above 0.13, however, the short-range structure around Mn approaches more and more that of groutite, while the short-range structure around Fe remains goethite-like. Assuming a statistical distribution of 10% Mn over all 4c sites, the probability of having two Mn atoms neighboring each other is $0.1^2 = 0.01$, and that of having Mn sur-

TABLE 3. Summary of XAFS data fitting for Mn*K*α

	1st Mn-Me (CN = 2)		2nd Mn-Me (CN = 2)		3rd Mn-Me (CN = 4)			
x_{Mn}	*R* (Å)	σ² (Å²)	*R* (Å)	σ² (Å²)	*R* (Å)	σ² (Å²)	ΔE_0	χ^2_{res}
0.05	3.00	0.0013	3.20	0.0040	3.41	0.0055	–1.1	9.9
0.13	3.00	0.0014	3.22	0.0046	3.40	0.0031	–3.2	8.9
0.18	2.96	0.0061	3.29	0.0035	3.49	0.0038	–0.3	4.0
0.35	2.92	0.0048	3.34	0.0039	3.54	0.0030	0.6	5.0
0.47	2.90	0.0043	3.32	0.0053	3.54	0.0040	0.3	6.1
1.00	2.86	0.0052	3.42	0.0061	3.59	0.0014	1.3	4.4

Notes: CN is coordination number, *R* is interatomic distance, σ² is the Debye-Waller factor, ΔE_0 is the phase shift, and χ^2_{res} is the goodness of fit. Uncertainties in *R* are ±0.01 Å (1st and 3rd shell) and ±0.03 Å (2nd shell).

TABLE 2. Summary of XAFS data fitting for Fe*K*α

	1st Fe-Me (CN = 2)		2nd Fe-Me (CN = 2)		3rdFe-Me (CN = 4)			
x_{Mn}	*R* (Å)	σ² (Å²)	*R* (Å)	σ² (Å²)	*R* (Å)	σ² (Å²)	ΔE_0	χ^2_{res}
0.00	3.00	0.0025	3.27	0.0055	3.42	0.0052	0.8	4.1
0.05	3.01	0.0027	3.28	0.0038	3.43	0.0040	0.4	5.2
0.13	3.01	0.0027	3.28	0.0046	3.43	0.0042	0.9	4.4
0.18	2.99	0.0040	3.27	0.0034	3.43	0.0048	–0.2	5.1
0.35	2.97	0.0044	3.28	0.0053	3.45	0.0053	0.2	6.3
0.47	2.97	0.0062	3.25	0.0106	3.46	0.0077	0.1	4.0

Notes: CN is coordination number, *R* is interatomic distance, σ² is the Debye-Waller factor, ΔE_0 is the phase shift, and χ^2_{res} is the goodness of fit. Uncertainties in *R* are ±0.01 Å (1st and 3rd shell) and ±0.03 Å (2nd shell).

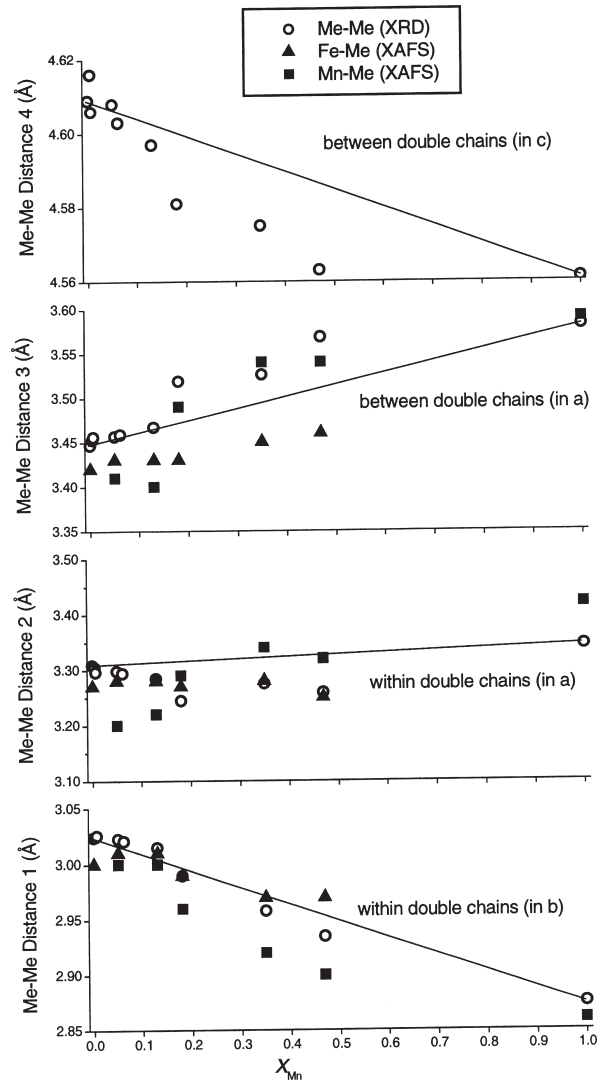

FIGURE 5. Rietveld-derived metal-metal distances and XAFS-derived iron-metal and manganese-metal distances. The lines link the end-member distances.

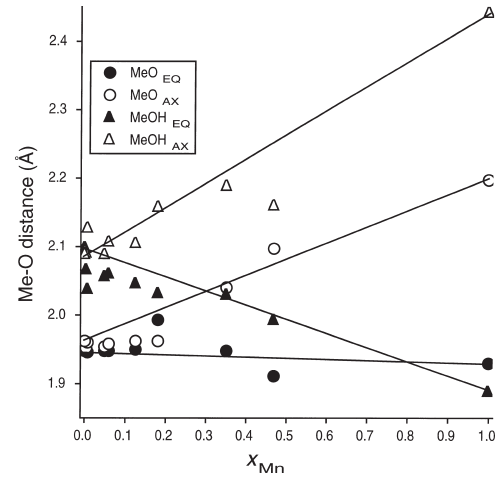

FIGURE 4. Rietveld-derived metal-oxygen distances. The lines link the end-member distances.

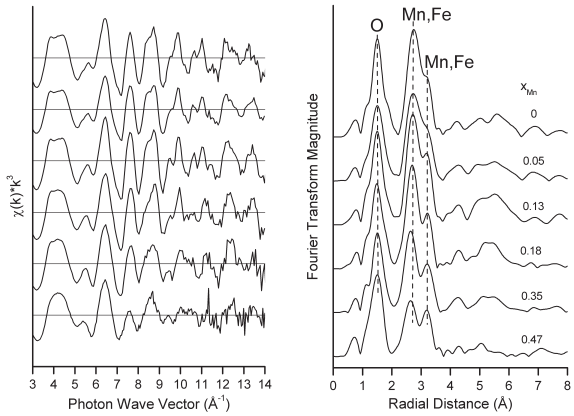

FIGURE 6. Fe*K*α XAFS spectra. The radial structure functions are uncorrected for phase shift.

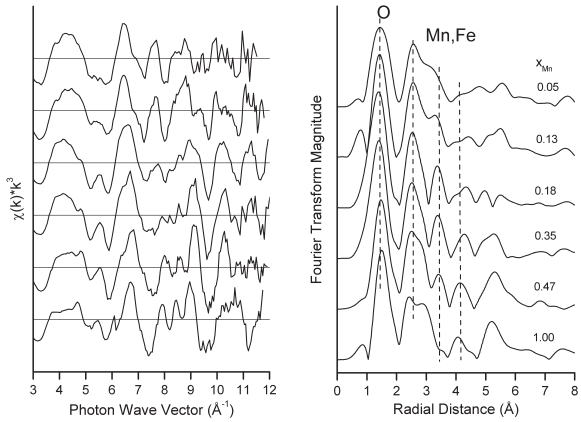

FIGURE 7. Mn*K*α XAFS spectra. The radial structure functions are uncorrected for phase shift.

rounded by Mn only (six Mn neighbors) is $0.1^7 = 10^{-7}$. This low probability of Mn forming clusters explains why the Mn environment is goethite-like at $x_{Mn} \leq 0.13$. However, even at $x_{Mn} = 0.20$ the probabilities remain extremely low (2 Mn: 0.04, 7 Mn: 1.28 10^{-5}). Therefore, the deviation between the Fe and the Mn environments above 0.13 suggest that Mn octahedra cluster more frequently than would be expected from a homogeneous distribution of Mn across the 4c sites in the goethite structure.

Such preferential clustering was reported for naturally occurring and man-made solid solutions (Waychunas 1983; Manceau and Calas 1985; Manceau 1990; Chmaissem et al. 1995). In Al-substituted goethite, the homogeneous distribution of Al across the 4c sites of goethite seems to be limited by the size mismatch between the smaller Al^{3+} and larger Fe^{3+} (Scheinost et al. 1999). Gasser et al. (1999) used an analytical transmission electron microscope to show that acicular goethite crystals of series Mni-* are composed of Mn-rich and Fe-rich zones. The driving force for the cluster formation is most likely the incompatibility between increasingly distorted $Mn(O,OH)_6$ octahedra and the more isotropic $Fe(O,OH)_6$ octahedra. The transition from a goethite-like to a groutite-like environment, which happens between x_{Mn} of 0.13 and 0.18, may

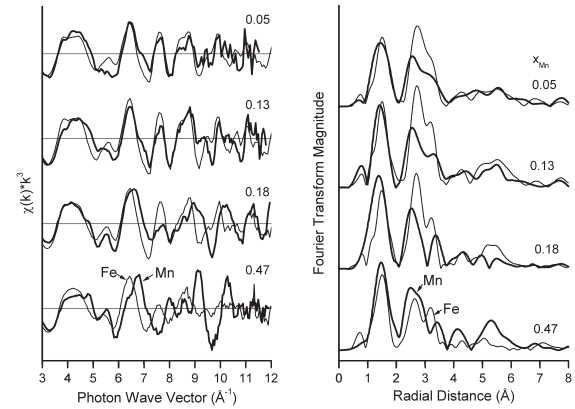

FIGURE 8. Comparison between Fe*K*α and Mn*K*α edge spectra of select Mn goethite samples.

indicate that a critical threshold value of x_{Mn} was exceeded. However, the samples above this threshold value are from one synthesis series (Ebinger and Schulze 1990). Therefore, the observed formation of groutite clusters may be either the effect of the level of Mn substitution, the effect of the specific synthesis procedure employed, or a combination of both. Most likely the synthesis procedure promoted the clustering which, in turn, allowed for the much higher Mn substitution as compared to the other series.

ACKNOWLEDGMENTS

A.C.S. acknowledges the Deutsche Forschungsgemeinschaft for the generous support during a two-year stay at Purdue University and the University of Delaware. This work was partially supported by U.S.D.A. National Research Initiative grant 96-35107-3183 to D.G.S., and by C.N.R.S. (France; URSSAF No. 540 547 171 861 and CIES grant no. 156249E) to U.G. Richard V. Morris, NASA, Houston, Texas, shared the samples of the MnGt* series, Peter Dunn, National Museum of Natural History, provided the groutite sample no. 138621, and Don Ross, University of Vermont, provided the Mn^{3+}-pyrophosphate. This is journal article number 16349 of the Purdue Office of Research Programs.

REFERENCES CITED

Ammundsen, B., Jones, D.J., Rozière, J., and Burns, G.R. (1996) Effect of chemical extraction of lithium on the local structure of spinel lithium manganese oxides determined by X-ray absorption spectroscopy. Chemistry of Materials, 8, 2799–2808.

Anand, R.R. and Gilkes, R.J. (1987) Iron oxides in lateritic soils from Western Australia. Journal of Soil Science, 38, 607–622.

Ankudinov, A.L. and Rehr, J.J. (1997) Relativistic spin-dependent X-ray absorption theory. Physical Review B, 56, 1712–1728.

Apte, M.Y. and Mande, C. (1982) Chemical effects on the main peak in the K absorption spectrum of manganese in some compounds. Journal of Physics C: Solid State Physics, 15, 607–613.

Bajt, S., Clark, S.B., Sutton, S.R., Rivers, M.L., and Smith, J.V. (1993) Synchrotron x-ray microprobe determination of chromate content using x-ray absorption near-edge structure. Analytical Chemistry, 65, 1800–1804.

Birnie, A.C. and Paterson, E. (1991) The mineralogy and morphology of iron and manganese oxides in an imperfectly-drained Scottish soil. Geoderma, 50, 219–237.

Boughriet, A., Ouddane, B., Wartel, M., Lalou, C., Cordier, C., Gengembre, L., and Sanchez, J.P. (1996) On the oxidation states of Mn and Fe in polymetallic oxide/oxyhydroxide crusts from the Atlantic Ocean. Deep-Sea Research I, 43, 321–343.

Burns, R.G. (1993) Mineralogical Applications of Crystal Field Theory. 551 p. Cambridge University Press.

Burns, V.M. and Burns, R.G. (1979) Observations of processes leading to the uptake of transition metals in manganese nodules. In C.N.d.l.R. Scientifique, Ed. La genèse des nodules de manganèse, 289, Gif-sur-Yvette.

Caglioti, G., Paoletti, A., and Ricci, F.P. (1958) Choice of collimators for a crystal spectrometer for neutron diffraction. Nuclear Instruments and Methods, 3, 223–226.

Calas, G., Manceau, A., and Petiau, J. (1988) Crystal chemistry of transition elements in minerals through X-ray absorption spectroscopy. In A. Barto-Kyriakidis, Ed. Synchrotron Radiation Applications in Mineralogy and Petrology, p. 77–95. Theophrastus Publications, S.A., Athens, Greece.

Carlson, L. (1995) Aluminum substitution in goethite in lake ore. Bull. Geol. Soc. Finland, 67, 19–28.

Chmaissem, O., Argyriou, D.N., Hinks, D.G., Jorgensen, J.D., Storey, B.G., Zhang, H., Marks, L.D., Wang, Y.Y., Dravid, V.P., and Dabrowski, B. (1995) Chromium clustering and ordering in $Hg_{1-x}Cr_xSr_2CuO_4$+delta. Physical Review B—Condensed Matter, 52, 15636–15643.

Cornell, R.M. and Giovanoli, R. (1987a) Effect of manganese on the transformation of ferrihydrite into goethite and jacobsite in alkaline media. Clays and Clay Minerals, 35, 11–20.

———(1987b) Effect of manganese on the transformation of ferrihydrite into goethite and jacobsite in alkaline media. Clays and Clay Minerals, 35, 11–20.

Dent Glasser, L.S. and Ingram, L. (1968) Refinement of the crystal structure of groutite, α-MnOOH. Acta Crystallographica, B 24, 1233–1236.

Diaz, C., Furet, N.R., Nikolaev, V.I., Rusakov, V.S., and Cordeiro, M.C. (1989) Mössbauer effect study of Co, Ni, Mn, and Al bearing goethites. Hyperfine Interactions, 46, 689–693.

Ebinger, M.H. and Schulze, D.G. (1989) Mn-substituted goethite and Fe-substituted groutite synthesized at acid pH. Clays and Clay Minerals, 37, 151–156.

———(1990) The influence of pH on the synthesis of mixed Fe-Mn oxide minerals. Clay Minerals, 25, 507–518.

Fabris, J.D., Resende, M., Allan, J., and Coey, J.M.D. (1986) Mössbauer analysis of Brazilian oxisols. Hyperfine Interactions, 29, 1093–1096.

Fitzpatrick, R.W. and Schwertmann, U. (1982) Al-substituted goethite—an indicator of pedogenic and other weathering environments in South Africa. Geoderma, 27, 335–347.

Ford, R.G., Bertsch, P.M., and Farley, K.J. (1997) Changes in transition and heavy metal partitioning during hydrous iron oxide aging. Environmental Science and Technology, 31, 2028–2033.

Forsyth, J.B., Hedley, I.G., and Johnson, C.E. (1968) The magnetic structure and hyperfine field of goethite (α-FeOOH). Journal of Physical Chemistry C, Ser. 2, Vol. 1, 179–188.

Fritsch, S., Post, J.E., and Navrotsky, A. (1997) Energetics of low-temperature polymorphs of manganese dioxide and oxyhydroxide. Geochimica et Cosmochimica Acta, 61, 2613–2616.

Gasser, U.G., Nüesch, R., Singer, M.J., and Jeanroy, E. (1999) Distribution of Mn in synthetic goethite. Clay Minerals, 34, 291–299.

Hoffmann, C., Armbruster, T., and Kunz, M. (1997) Structure refinement of (001) disordered gaudefroyite $Ca_4Mn_3^{3+}[(BO_3)_3(CO_3)O_3]$: Jahn-Teller-distortion in edge-sharing chains of $Mn^{3+}O_6$ octahedra. European Journal of Mineralogy, 9, 7–19.

Hus, J.J. and Stiers, W. (1987) The magnetic properties of an ironcrust in SE Belgium and synthetic Mn-substituted goethites. Physics of the Earth and Planetary Interiors, 46, 247–258.

Izumi, F. (1993) Rietveld analysis programs RIETAN and PREMOS and special applications. In R.A. Young, Ed. The Rietveld Method, p. 236–253. Oxford University Press, Oxford.

Junta, J.L. and Hochella, M.F. (1994) Manganese (II) oxidation at mineral surfaces: a microscopic and spectroscopic study. Geochimica et Cosmochimica Acta, 58, 4985–4999.

Manceau, A. (1990) Distribution of cations among the octahedra of phyllosilicates: Insight from EXAFS. Canadian Mineralogist, 28, 321–328.

Manceau, A. and Calas, G. (1985) Heterogeneous distribution of nickel in hydrous silicates from New Caledonia ore deposits. American Mineralogist, 70, 549–558.

Manceau, A., Gorshkov, A.I., and Drits, V.A. (1992) Structural chemistry of Mn, Fe, Co, and Ni in manganese hydrous oxides: Part I. Information from XANES spectroscopy. American Mineralogist, 77, 1133–1143.

Mandernack, K.W., Post, J., and Tebo, B.M. (1995) Manganese mineral formation by bacterial spores of the marine Bacillus, strain SG-1: evidence for the direct oxidation of Mn(II) to Mn(IV). Geochimica et Cosmochimica Acta, 59, 4393–4408.

Mason, B. and Moore, C. (1982) Principles of Geochemistry. 344 p. John Wiley & Sons, New York.

Murray, J.W., Dillard, J.G., Giovanoli, R., Moers, H., and Stumm, W. (1985) Oxidation of Mn(II): Initial mineralogy, oxidation state and ageing. Geochimica et Cosmochimica Acta, 49, 463–470.

Nesbitt, H.W. and Banerjee, D. (1998) Interpretation of XPS Mn(2p) spectra of Mn oxyhydroxides and constraints on the mechanism of MnO_2 precipitation. American Mineralogist, 83, 305–315.

Patrick, W.H. Jr. and Jugsujinda, A. (1992) Sequential reduction and oxidation of inorganic nitrogen, manganese, and iron in flooded soil. Soil Science Society of America Journal, 56, 1071–1073.

Riggs-Gelasco, P.J., Mei, R., Ghanotakis, D.F., Yocum, C.F., and Penner-Hahn, J.E. (1996) X-ray absorption spectroscopy of calcium-substituted derivatives of the oxygen-evolving complex of photosystem II. Journal of the American Chemical Society, 118, 2400–2410.

Robbins, E.I., D'Agostino, J.P., Ostwald, J., Fanning, D.S., Carter, V., and Van Hoven, R. (1993) Manganese nodules and microbial oxidation of manganese in the Huntley Meadows wetland, Virginia, USA. In H.C.W. Skinner, and R.W. Fitzpatrick, Eds. Biomineralization. Processes of iron and manganese—Modern and ancient environments, 21, p. 179–202. Catena Verlag, Cremlingen, Germany.

Ross, S.J. Jr., Franzmeier, D.P., and Roth, C.B. (1976) Mineralogy and chemistry of manganese oxides in some Indiana soils. Soil Science Society of America Journal, 40, 137–143.

Scheinost, A.C., Schulze, D.G., and Schwertmann, U. (1999) Diffuse reflectance spectra of Al substituted goethite: A ligand field approach. Clays and Clay Minerals, 47, 156–164.

Schulze, D.G. and Schwertmann, U. (1984) The influence of aluminium on iron oxides: X. Properties of Al-substituted goethites. Clay Minerals, 19, 521–529.

Schulze, D.G., Sutton, S.R., and Bajt, S. (1995) Determining manganese oxidation state in soils using X-ray absorption near-edge structure (XANES) spectroscopy. Soil Science Society of America Journal, 59, 1540–1548.

Schwertmann, U. and Pfab, G. (1997) Structural vanadium and chromium in lateritic iron oxides: genetic implications. Geochimica et Cosmochimica Acta, 60, 4279–4283.

Schwertmann, U., Cambier, P., and Murad, E. (1985) Properties of goethites of varying crystallinity. Clays and Clay Minerals, 33, 369–378.

Silvester, E., Manceau, A., and Drits, V.A. (1997) Structure of synthetic monoclinic Na-rich birnessite and hexagonal birnessite: II. Results from chemical studies and EXAFS spectroscopy. American Mineralogist, 82, 962–978.

Singh, B. and Gilkes, R.J. (1992) Properties and distribution of iron oxides and their association with minor elements in the soils of south-western Australia. Journal of Soil Science, 43, 77–98.

Stiers, W. and Schwertmann, U. (1985) Evidence for manganese substitution in synthetic goethite. Geochimica et Cosmochimica Acta, 49, 1909–1911.

Stumm, W. and Morgan, J.J. (1970) Aquatic Chemistry. Wiley, New York.

Tardy, Y. and Nahon, D. (1985) Geochemistry of laterites. Stability of Al-goethite, Al-hematite and Fe^{3+}-kaolinite in bauxites and ferricretes. An approach to the mechanism of concretion formation. American Journal of Science, 285, 865–903.

Taylor, R.M., McKenzie, R.M., and Norrish, K. (1964) The mineralogy and chemistry of manganese in some Australian soils. Australian Journal of Soil Research, 2, 235–248.

Thompson, P., Cox, D.E., and Hastings, J.B. (1987) Rietveld refinement of Debye-Scherrer synchrotron X-ray data from Al_2O_3. Journal of Applied Crystallography, 20, 79–83.

Trolard, F., Bourrie, G., Jeanroy, E., Herbillon, A.J., and Martin, H. (1995) Trace metals in natural iron oxides from laterites: a study using selective kinetic extraction. Geochimica et Cosmochimica Acta, 59, 1285–1297.

Trolard, F., Francois, M., and Martin, H. (1989) Localisation des éléments-traces et contrìle cinétique de la dissolution sélective de phases minérales dans les latérites. Comptes Rendus de l'Académie des Sciences, Paris, 308, 401–406.

Tu, S., Racz, G.J., and Goh, T.B. (1994) Transformation of synthetic birnessite as affected by pH and manganese concentration. Clays and Clay Minerals, 42, 321–330.

Uzochukwu, G.A. and Dixon, J.B. (1986) Manganese oxide minerals in nodules of two soils of Texas and Alabama. Soil Science Society of America Journal, 50, 1358–1363.

Vandenberghe, R.E., DeGrave, E., DeGeyter, G., and Landuydt, C. (1986a) Characterization of goethite and hematite in a Tunisian soil profile by Mössbauer spectroscopy. Clays and Clay Minerals, 34, 275–280.

Vandenberghe, R.E., Verbeeck, A.E., De Grave, E., and Stiers, W. (1986b) ^{57}Fe Mössbauer effect study of Mn-substituted goethite and hematite. Hyperfine Interactions, 29, 1157–1160.

Varentsov, I.M. (1996) Manganese Ores of Supergene Zone: Geochemistry of Formation. 342 p. Kluwer Academic Publishers, Dordrecht.

Vempati, R.K., Morris, R.V., Lauer, H.V., and Helmke, P.A. (1995) Reflectivity and other physicochemical properties of Mn-substituted goethites and hematites. Journal of Geophysical Research, 100, 3285–3295.

Waychunas, G.A. (1983) Mössbauer, EXAFS and X-ray diffraction study of the Fe^{3+} clusters in MgO:Fe and magnesiowüstite $(Mg,Fe)_{1-x}O$—Evidence for specific cluster geometries. Journal of Material Science, 18, 195–207.

Wolski, W., Wolska, E., Kaczmarek, J., and Piszora, P. (1997) Ferrimagnetic spinels in hydrothermal and thermal treatment of $Mn_xFe_{2-2x}(OH)_{6-4x}$. Journal of Thermal Analysis, 48, 247–258.

MANUSCRIPT RECEIVED NOVEMBER 16, 1999
MANUSCRIPT ACCEPTED AUGUST 10, 2000
PAPER HANDLED BY H. WAYNE NESBITT